Mechanical Systems and Signal Processing 81 (2016) 294–307

Contents lists available at ScienceDirect

Mechanical Systems and Signal Processing

journal homepage: www.elsevier.com/locate/ymssp

Estimation of impact damping parameters for a cam–follower system based on measurements and analytical model

Sriram Sundar, Jason T. Dreyer, Rajendra Singh *

Acoustics and Dynamics Laboratory, Smart Vehicle Concepts Center, Department of Mechanical and Aerospace Engineering, The Ohio State University, Columbus, OH 43210, USA

ARTICLE INFO

Article history:
Received 16 July 2015
Received in revised form
25 January 2016
Accepted 9 February 2016
Available online 18 March 2016

Keywords:
Cam–follower system dynamics
Non-linear contact dynamics
Time-domain signal processing
Coefficient of restitution

ABSTRACT

A new cam–follower system experiment capable of generating periodic impacts is utilized to estimate the impact damping model parameters. The experiment is designed to precisely measure the forces and acceleration during impulsive events. The impact damping force is described as a product of a damping coefficient, the indentation displacement raised to the power of a damping index, and the time derivative of the indentation displacement. A novel time-domain based technique and a signal processing procedure are developed to accurately estimate the damping coefficient and index. The measurements are compared to the predictions from a corresponding contact mechanics model with trial values of damping parameters on the basis of a particular residue; both parameters are quantified based on the minimization of this residue. The estimated damping parameters are justified using the literature and an equivalent coefficient of restitution model is developed. Also, some unresolved issues regarding the impact damping model are addressed.

1. Introduction

Periodic impacts commonly occur in mechanical systems having clearance or backlash; these include geared systems [1–5], cam–follower mechanisms [6–9], and four-bar linkages [10–12]. There is a significant body of literature on such impacting systems employing linear system methods [13,14], non-linear analysis [15], stability investigations [16–18] and energy dissipation analyses [19,20]. However, only a few researchers [15,21,22] have utilized contact mechanics formulation (with an impact damping model) for such systems. The commonly used contact force formulation [21,23–25] is of the following form,

$$F_\lambda = F_k\left(1+\kappa\dot{\delta}\right). \tag{1}$$

Here, F_λ is the contact force (where subscript λ indicates a contact related parameter), F_k is the contact stiffness force, δ is the indentation displacement, and κ is an arbitrary constant. The physical significance of the above formulation is that the contact damping force is assumed to be proportional to the elastic contact force. Additionally, an alternate formulation such as $F_\lambda = F_k+\eta\delta^{0.25}\dot{\delta}$ (where η is a constant) has also been used [22] to represent the contact force during impacts. Overall, there is a clear need to experimentally determine the most appropriate impact damping model, though the direct

* Corresponding author. Tel.: +1 614 292 9044.
E-mail address: singh.3@osu.edu (R. Singh).

http://dx.doi.org/10.1016/j.ymssp.2016.02.033
0888-3270/

measurement of contact force during an impact remains a challenge. Therefore, the main goal of this article is to propose a new method that would combine measurements and analytical predictions for a cam–follower system to estimate impact damping parameters.

2. Problem formulation

A generalized model for the contact force is proposed below where n is the damping index and β is the impact damping coefficient.

$$F_\lambda = F_k + \beta\delta^n\dot{\delta} \tag{2}$$

The above formulation does not assume a proportionality between the contact stiffness and damping forces. A limiting case of this equation, however, is when the n is equal to the power of δ in F_k, then F_d is proportional to F_k. The extent of hysteresis is controlled by the value of n. Note that the β units depend on the numerical value of n since $\beta\delta^n\dot{\delta}_i$ must have the units of force. The Hertzian contact theory [26] could be used to find F_k since it gives a reasonable estimate of the elastic force as suggested by Veluswami et al. [23]. The values of β and n could then be experimentally determined, though only a limited number of researchers [27] have conducted experimental studies using an impact damping model. Nevertheless, the following key questions remain unanswered: a) will Eq. (2) with experimentally estimated values of β and n be consistent with Eq. (1)? b) Could the hysteresis loop and the contact force be utilized to estimate β and n? c) What is the relative significance of the numerical values of β and n? d) How could one justify the numerical values of β and n, given the literature for a typical mechanical system? e) Is the equivalent viscous damping model appropriate for this problem? Therefore, the scope of this study is formulated to address the above mentioned questions, though it is restricted to impacts with point contacts between two metallic objects.

The key objectives of this article are as follows: (i) design a controlled cam–follower experiment with point contact to measure dynamic forces and motion (in time domain) under periodic impacts; (ii) propose an analogous analytical model for the experiment with contact mechanics formulation; (iii) develop and evaluate a signal processing procedure to experimentally determine β and n without directly measuring the contact force; and (iv) determine an equivalent coefficient of restitution model from the same experiment, and then justify the estimated value(s) of β using the relationship suggested by Hunt and Crossley [24].

The cam–follower system proposed for this study is shown in Fig. 1, which is a representative experiment for impacting mechanical systems, as shown previously [22]. The system consists of a cylindrical steel cam rotating about an axis not passing through its center but parallel to the axis of the cylinder. The follower consists of a long bar of square cross-section attached to a thin cylindrical steel dowel pin, pivoted at its end by a pair of roller bearings, and supported along the vertical direction ($\hat{e}_y$) by a coil spring which is always compressed, thereby forcing it towards the rotating cam. The main assumptions regarding the experiment are: a) the axes of rotation of the cam and the follower remain unchanged at any load; b) the bearings at the follower pivot are frictionless; c) the angular velocity of the cam (Ω_c, subscript c denoting the cam) is constant and unaffected by the impact loads; and d) the coil spring stays vertical during the operation. The following conditions are to be considered in designing the cam–follower experiment to achieve a good estimate of β and n. First, the effect of flexural vibrations of the follower caused by impacts should not affect the measured force and acceleration. Second, the responses should be accurately measured during the impacts which occur within a very short time interval. Finally, the follower must impact with the cam periodically at the rate of once per cam revolution; the need to have this particular condition is explained in Section 5.

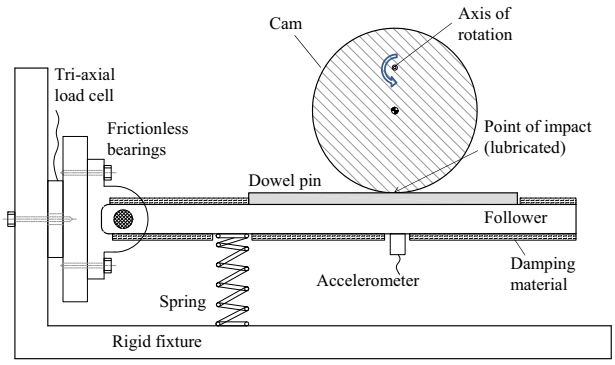

Fig. 1. Cam–follower experiment designed to determine impact damping parameters.

3. Design of the laboratory experiment and instrumentation

The cam–follower experiment is designed as follows for accurate estimation. First, a point contact is achieved between the cam (of radius r_c, subscript c denoting the cam) and the dowel pin (of radius r_d) of the follower, since two cylindrical surfaces (with axes perpendicular to each other) are in contact. Second, the coefficient of friction (μ) is minimized by having smooth contacting surfaces (with an average roughness of 0.2 μm). At the contact, μ is taken to be as 0.2, though this value does not influence the estimation procedure. Third, the flexural vibrations in the follower (of width w_b, subscript b denoting the bar) are minimized using a damping material (Sika damp 620 [28]). Fourth, a tri-axial force transducer (PCB 260A01 [29]) located at the follower hinge measures the reaction forces along $\hat{e}_x$ (horizontal) and $\hat{e}_y$ directions, while the shock accelerometer (PCB 350B02 [30]) attached to the follower near the contact point (at a distance of l_a from the follower pivot) measures its tangential acceleration. Both transducers (capable of accurately recording the impacts) are simultaneously sampled at a very high rate of 204800 Hz using the LMS Scadas III [31] data acquisition system. Finally, the contact is maintained when Ω_c is low; however, the follower (of length l_b) starts losing contact and making impacts as Ω_c is increased considerably. As observed by Alzate et al. [8], the system quickly goes into a chaotic state once Ω_c is increased beyond a certain limit. Hence, a variable speed electric motor is used to carefully control Ω_c, so that the system does a periodic impact of exactly once per revolution of the cam. As Ω_c is slowly increased, the time period between consecutive impacts increases while the time period for the cam to complete one revolution decreases. The follower impacts exactly once per cam's revolution when these two time periods are equal. A digital tachometer (Neiko Tools, USA) is used to accurately measure Ω_c.

4. Analytical model

4.1. Kinematics of the cam–follower system

Fig. 2 shows a sketch of the analytical model with a contact mechanics formulation for the experiment. The cylindrical cam rotates about E which is at a distance e from the center (G_d). The linear stiffness of the coil spring supporting the bar is k_s and it is grounded at a distance d_y below the bearing pivot P and at a distance of d_x from it along $\hat{e}_x$. The angle made by the follower with $\hat{e}_x$ is given by $\alpha(t)$ measured in the clockwise direction, while the angular displacement of the cam in the counter-clockwise direction is given by $\Theta(t)$. The instantaneous points of contact in the cam and the follower are given by O_c and O_b, respectively. A moving coordinate system $\left(\hat{i},\hat{j}\right)$ attached to the follower is defined with its origin at Q where $\hat{i}$ is orthogonal to the follower. The vector $\overrightarrow{QO_c}$ in the $\left(\hat{i},\hat{j}\right)$ coordinate system is given by $\psi_i\hat{i}+\psi_j\hat{j}$ as shown in Fig. 2. The 0-state is defined with Θ^0 and α^0 (with superscript 0 representing the 0-state), as discussed by Sundar et al. [9] for a similar system. The contact mechanics are represented by point contact stiffness (k_λ) and impact damping (c_λ) elements. The chief assumptions in the analytical formulation are as follows: (1) the friction does not affect the impact mechanism and it follows a Coulomb friction model; (2) the coil spring supporting the follower is linear; and (3) the bending moment in the

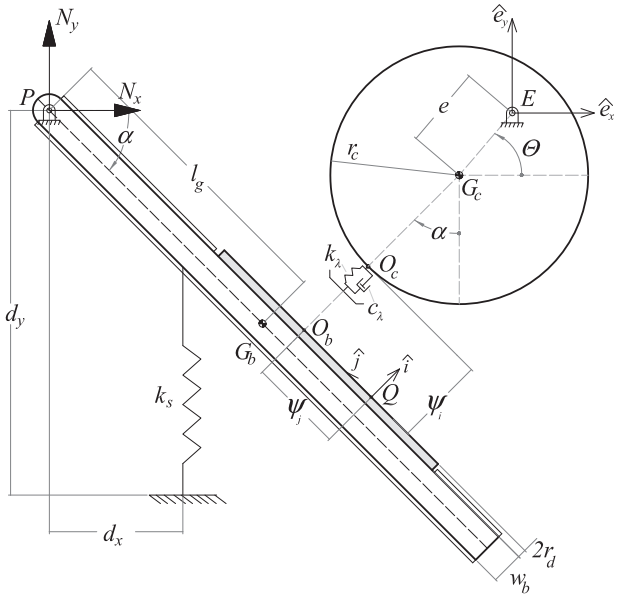

Fig. 2. Analytical contact mechanics model of the experiment shown in Fig. 1.

follower is negligible, furthermore the amplitude of flexural vibrations are negligibly small compared to the amplitude of angular oscillations due to impact.

At the 0-state, $\alpha^0$and $\Theta^0$are defined as the following,

$$\alpha^0 = \cos^{-1}\left(\frac{\sqrt{\left|\overrightarrow{PE}\right|_x^4+\left|\overrightarrow{PE}\right|_x^2\left|\overrightarrow{PE}\right|_y^2-\left|\overrightarrow{PE}\right|_x^2(0.5w_b+2r_d+r_c+e)^2}+\left|\overrightarrow{PE}\right|_y(0.5w_b+2r_d+r_c+e)}{\left|\overrightarrow{PE}\right|_x^2+\left|\overrightarrow{PE}\right|_y^2}\right), \tag{3}$$

$$\Theta^0 = \pi/2-\alpha^0. \tag{4}$$

Here $\left|\overrightarrow{PE}\right|_x$ and $\left|\overrightarrow{PE}\right|_x$ are the magnitudes of $\overrightarrow{PE}$ along $\hat{e}_x$ and $\hat{e}_y$, respectively. Using the procedure discussed by Sundar et al. [9], the moving coordinates ($\psi_i(t)$ and $\psi_j(t)$) and their time derivatives are calculated using the following equations:

$$\psi_i(t) = \chi^0\ \sin(\alpha(t)-\alpha^0)+(r_c+2r_d+0.5w_b)(\cos(\alpha(t)-\alpha^0)-1) + e\left[\sin\left(\alpha(t)+\Theta^0\right)-\ \sin(\alpha(t)+\Theta(t))\right], \tag{5}$$

$$\psi_j(t) = \chi^0\left[1-\ \cos(\alpha(t)-\alpha^0)\right]+(r_c+2r_d+0.5w_b)\sin(\alpha(t)-\alpha^0) - e\left[\cos\left(\alpha(t)+\Theta^0\right)-\ \cos(\alpha(t)+\Theta(t))\right], \tag{6}$$

$$\dot{\psi}_i(t) = \chi^0\ \cos(\alpha(t)-\alpha^0)\dot{\alpha}(t)-(r_c+2r_d+0.5w_b)\sin(\alpha(t)-\alpha^0)\dot{\alpha}(t) + e\left[\cos\left(\alpha(t)+\Theta^0\right)\dot{\alpha}(t)-\ \cos(\alpha(t)+\Theta(t))\left(\dot{\alpha}(t)+\dot{\Theta}(t)\right)\right], \tag{7}$$

$$\dot{\psi}_j(t) = \chi^0\ \sin(\alpha(t)-\alpha^0)\dot{\alpha}(t)+(r_c+2r_d+0.5w_b)\cos(\alpha(t)-\alpha^0)\dot{\alpha}(t) + e\left[\sin\left(\alpha(t)+\Theta^0\right)\dot{\alpha}(t)-\ \sin(\alpha(t)+\Theta(t))\left(\dot{\alpha}(t)+\dot{\Theta}(t)\right)\right]. \tag{8}$$

Here, $\chi^0=\chi(t)+\psi_j(t)$ where $\chi(t)$ is the lever arm of the $F_\lambda(t)$ about P and is given by the instantaneous magnitude of $\overrightarrow{PO_b}$ along $\hat{j}$.

4.2. Non-contact regime

When the instantaneous value of $\psi_i(t)>0$ the follower is not in contact with the cam, and the equation of motion depends only on the dynamics of the follower and coil spring. It is given by the following, where I_b^P is the moment of inertia of the follower (along with the damping material) about P, m_b is the mass of the follower (along with the damping material), and l_b is the distance from the center of gravity of the follower (G_b) from P:

$$I_b^P\ddot{\alpha}(t) = m_b g l_g\ \cos(\alpha(t))-F_s(t)d_x. \tag{9}$$

Here, $F_s(t)$ is the elastic force from the coil spring which is given as follows, where L_s^u is the undeflected length of the spring,

$$F_s(t) = k_s\left[L_s^u-d_y+d_x\ \tan(\alpha(t))+0.5w_b\ \sec(\alpha(t))\right]. \tag{10}$$

Eq. (9) is solved numerically for a given value of Ω_c, as long as $\psi_i(t)>0$. The system goes to a contact regime once $\psi_i(t)$ goes less than 0 and the response of the system has to be calculated using the contact mechanics formulation, which is discussed next.

4.3. Contact regime

Using the contact mechanics formulation, the response of the system is calculated using Hertzian contact theory [26]. The contact stiffness for a point contact is calculated as,

$$k_\lambda(\psi_i(t)) = \frac{4}{3}Y^e\left(\rho^e|\psi_i(t)|\right)^{0.5}. \tag{11}$$

Here Y is Young's modulus (with superscript e denoting equivalent) given by the following, where ν is Poisson's ratio,

$$Y^e = \left[\frac{1-\nu_c^2}{Y_c}+\frac{1-\nu_b^2}{Y_b}\right]^{-1}. \tag{12}$$

The equivalent radius of curvature at the contact (ρ^e) is given by,

$$\rho^e = \left[(r_c)^{-1}+(r_d)^{-1}\right]^{-1}. \tag{13}$$

The impact damping is defined as given below, as a direct result of the proposed generalized model given in Eq. (2),

$$c_\lambda(\psi_i(t)) = \beta|\psi_i(t)|^n. \tag{14}$$

The total contact force is given by,

$$F_\lambda(t) = -k_\lambda(\psi_i(t))\,\psi_i(t) - c_\lambda(\psi_i(t))\,\dot{\psi}_i(t). \tag{15}$$

Taking the moment balance of the forces acting on the follower about P, the equation of motion in the contact regime is calculated as,

$$I_b^P\ddot{\alpha}(t) = m_b g l_g\,\cos(\alpha(t)) - F_s(t)d_x + F_\lambda(t)\chi(t) - F_f(t)(0.5w_b + 2r_d). \tag{16}$$

Here $F_f(t)$ is the friction force given by

$$F_f(t) = \mu F_\lambda(t)\ \mathrm{sgn}(v_r(t)). \tag{17}$$

Here $v_r(t)$ is the relative sliding velocity at the contact point given by

$$v_r(t) = \dot{\psi}_j(t) - [r_c + e\,\sin(\alpha(t)+\Theta(t))]\left(\dot{\alpha}(t)+\dot{\Theta}(t)\right) \tag{18}$$

Note that from Eq. (16), $F_f(t)$ does not significantly affect the dynamics of the system as its moment arm $(0.5w_b+2r_d)$ is very small compared to $\chi(t)$, and moreover μ is very low. The system response is computed in the non-contact regime by solving Eq. (9), while in the contact regime by solving Eq. (16). The system constantly switches between these two regimes when Ω_c is greater than a certain value, depending on the system. At the very beginning of the simulation $\alpha(0)=\alpha^*$ and $\dot{\alpha}(0)=0$ are used as initial conditions, where α^* is the value of $\alpha(t)$ at the static equilibrium point (with superscript *). This is evaluated using Eqs. (5), (6) and (16) in the Jacobian matrix method as discussed by Sundar et al. [9]. Subsequently, the initial conditions for each regime are taken from the final state of the previous regime.

5. Estimation of impact damping parameters (β and n)

5.1. Time-domain based technique to estimate the system response

The reaction forces along $\hat{e}_x$ and $\hat{e}_y$ (N_x and N_y, respectively, as shown in Fig. 2) and $\ddot{\alpha}(t)$ (calculated by dividing the measured tangential acceleration of the follower by l_a) are the experimental data measured in the time-domain. The geometrical parameters and inertia are obtained directly from the experiment. The entire procedure is performed in the time-domain as impacts excite a wide range of frequencies (including the natural frequencies of the cam–follower system and flexural vibrations of the follower), and hence the frequency domain data cannot be used directly. Some of the important numerical issues for which care needs to be taken in this estimation process are as follows. First, the measured $\ddot{\alpha}(t)$ is numerically integrated to obtain $\dot{\alpha}(t)$, which is numerically integrated again to obtain the system response ($\alpha(t)$). The integration process does not give the DC component of the signal; moreover the numerical integration process has inherent errors [32] (truncation and round-off) associated with it. Also since integration has to be performed twice, these errors would have a cumulative effect on $\alpha(t)$. Thus, higher accuracies can be achieved by having a shorter time resolution (τ) and a smaller length of integration vector. Second, the magnitude of indentation ($\psi_i(t)$) during contact is very small compared to the maximum value of $\alpha(t)$ in the non-contact regime and the time of impact is very short. Hence it is very difficult to accurately estimate $\psi_i(t)$ during impacts from the experimental data.

The following technique is adopted to minimize the errors due to the numerical integration and to estimate the DC component of $\alpha(t)$. The impact damping estimation procedure discussed later in Section 5.2 can be employed even without adopting this technique, if $\alpha(t)$ can be accurately calculated from the experiment. The measured time-domain data (forces and acceleration) have many impacts, but each impact is considered an independent event for the purpose of analysis. Furthermore, each impact event is divided into two sub-events, namely contact and non-contact. The contact sub-event begins when the cam and the follower are just in contact ($t^i=0$, superscript i represents experimental data for an impact event) with $\psi_i^i=0$ and ends when the follower loses contact with the cam ($t^i=t_a^i$). Then the non-contact sub-event starts and lasts until the follower next comes into contact with the cam ($t^i=t_e^i$). The experimental angular acceleration for each impact event is measured as $\ddot{\alpha}^i(t^i)$ and its time-average $\left(\left\langle\ddot{\alpha}^i(t^i)\right\rangle_{t^i}\right)$ should be 0 since the impacts are periodic (as stated in Section 3). However, this is not generally the case as the measured data has some errors, and hence $\left\langle\ddot{\alpha}^i(t^i)\right\rangle_{t^i}$ is subtracted from $\ddot{\alpha}^i(t^i)$. Then $\ddot{\alpha}^i(t^i)$ is integrated numerically using the Runge–Kutta method to get $\dot{\alpha}^i(t^i)$. Though $\left\langle\ddot{\alpha}^i(t^i)\right\rangle_{t^i}$ should be 0, it is not due to the errors of the numerical integration technique. This is eliminated by subtracting $\left\langle\dot{\alpha}^i(t^i)\right\rangle_{t^i}$ from $\dot{\alpha}^i(t^i)$. The resultant signal is again integrated numerically to get $\alpha^i(t^i)$. The fact that the follower impacts exactly once per revolution of the cam is used again to calculate the DC component of $\alpha^i(t^i)$. For a given system, the time period of each impact (t_e^i) depends on its state at the end of the contact sub-event. Writing it mathematically as follows where Ξ is a function that

gives the time required by the follower to return to its initial position based on initial conditions,

$$t_e^i = \Xi\left(\alpha^i(t_a^i), \dot{\alpha}^i(t_a^i)\right). \tag{19}$$

Eq. (9) is solved iteratively with known $\dot{\alpha}^i(t_a^i)$ and different values of α as initial condition to evaluate Ξ. The time required for the follower to come back to the same initial position is calculated for each α. The value of α, for which the calculated time matches with t_e^i, is chosen as $\alpha^i(t_a^i)$ since $t_a^i \approx 0$ (due to extremely short time of contact sub-event). The DC component of $\alpha^i(t^i)$ (calculated by numerical integration) is adjusted so that $\alpha^i(t^i)|_{t^i = t_a^i} = \alpha^i(t_a^i)$. The angle of the cam at $t^i = 0$ $\left(\Theta^i(0)\right)$ is calculated from Eq. (5) by replacing $\alpha(t)$ with $\alpha^i(0)$ $\alpha^i(0)$, forcing $\psi_i(t) = 0$ and solving for $\Theta(t)$. Thus the time-history of Θ can be calculated as,

$$\Theta^i\left(t^i\right) = \Theta^i(0) + \Omega_c\left(t^i\right) \tag{20}$$

5.2. Signal processing procedure used to estimate β and n

It is not possible to have a direct method to estimate the impact damping parameters because of their inter-relationship with the measured acceleration and reaction forces. Hence they are identified using an indirect method of comparing the experimental data for each impact with the results from an analytical model with trial values of β and n which is defined as simulation S_1 (where S_1 represents simulation with trial values). To aid in the comparison process, the $F_\lambda^i(t^i)$ during contact $(0 < t^i < t_a^i)$ is calculated from the measured data using the force balance as,

$$F_\lambda^i(t^i) = m_b l_g \ddot{\alpha}(t^i) + N_x^i(t^i)\sin\left(\alpha^i(t^i)\right) + \left[N_y^i(t^i) + F_s^i(t^i) - m_b g\right]\cos\left(\alpha^i(t^i)\right) \tag{21}$$

Here $F_s^i(t^i)$ is calculated from Eq. (10) by replacing $\alpha(t)$ with $\alpha^i(t^i)$. Also the maximum amplitude of response (α_m^i) is calculated as the following where 'max' is a function that returns the maximum value of a set of inputs,

$$\alpha_m^i = \max\left(\alpha^i(t^i)\right) \tag{22}$$

The results of simulation S_1 are obtained for each impact event by solving the equations of motion of the contact sub-event (Eq. (16)) with $\alpha^i(0)$ and $\dot{\alpha}^i(0)$ as initial conditions from the experimental data of the impact event, followed by the equation of motion in the non-contact sub-event (Eq. (9)) until $t^{S_1} = t_e^i$ (superscript S_1 represents results with simulation S_1 with trial values of β and n for the corresponding impact event). Simulation S_1 is conducted using different trial values of β and n for each impact event to compare with the experimental results. Similar to the experimental results $F_\lambda^{S_1}(t^{S_1})$, $\psi_i^{S_1}(t^{S_1})$ and $\alpha_m^{S_1}$ are estimated for each simulation. For the purpose of comparing the experimental results with that of simulation S_1 three different residues are formulated and analyzed (for error and sensitivity) to pick the best residue for the parameter evaluation. The residues are defined as follows:

$$\Lambda_1 = \frac{\left|\alpha_m^{S_1} - \alpha_m^i\right|}{\alpha_m^i}, \tag{23a}$$

$$\Lambda_2 = \frac{\sqrt{\int_0^{t_e^i}\left(F_\lambda^i(t) - F_\lambda^{S_1}(t)\right)^2.dt}}{\sqrt{\int_0^{t_e^i}\left(F_\lambda^i(t)\right)^2.dt}}, \tag{23b}$$

$$\Lambda_3 = \frac{\left|\oint F_\lambda^i(\psi_i^i).d(\psi_i^i) - \oint F_\lambda^{S_1}(\psi_i^{S_1}).d(\psi_i^{S_1})\right|}{\oint F_\lambda^i(\psi_i^i).d(\psi_i^i)} \tag{23c}$$

The maximum response of the system after the impact is the criterion considered for the first residue (Λ_1). The second residue (Λ_2) is based on the root mean square difference in the contact forces from the experiment and the simulated data in time-domain, while the third residue (Λ_3) uses the area under the hysteresis loop. The appropriate numerical values for β and n are identified based on the impact damping model which gives the minimum value of the average of the residues of all impact events. The estimation procedure can be based on either of the residues. Hence the accuracy of the estimation process using these residues will be discussed in Section 6.

The overall process of estimating β and n is described below as a step-by-step procedure.

Step 1: Accurate time histories of $\alpha^i(t^i)$, $\dot{\alpha}^i(t^i)$ and $\ddot{\alpha}^i(t^i)$ are obtained by adopting the signal processing procedure as explained in Section 5.1. Step 2: The contact force from the experiment $(F_\lambda^i(t^i))$ is calculated using Eq. (21). Step 3: Some trial values of β and n are assumed. Step 4: Response of simulation S_1 is obtained with the $\alpha^i(0)$ and $\dot{\alpha}^i(0)$ as initial conditions, (for contact sub-events and then the non-contact sub-event) to estimate $F_\lambda^{S_1}(t^{S_1})$, $\psi_i^{S_1}(t^{S_1})$ and $\alpha_m^{S_1}$. Step 5: Steps 3 and 4 are repeated for various trial values of β and n. Step 6: Best residue (among Λ_1, Λ_2 and Λ_3) is chosen based on error and sensitivity analyses (as explained in Section 6). Step 7: The measurement dataset is compared with the results of a different

Table 1
Selected parameters for the cam–follower experiment.

Parameter	Numerical value and units
m_b	0.257 kg
r_c	17.5 mm
I_b	3300 kg mm^2
l_g	173 mm
l_a	63 mm
l_b	86 mm
w_b	12.7 mm
r_d	3.2 mm
k_s	3319 N/m
L_s^u	53 mm
d_x	35 mm
d_y	58 mm
$\overrightarrow{PE}$	89 mm $\hat{e}_x$ + 27 mm $\hat{e}_y$
Y_c, Y_b	210 GPa
ν_c, ν_b	0.3

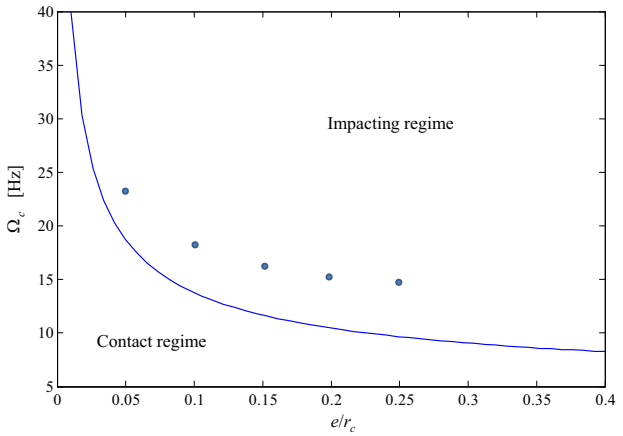

Fig. 3. Regimes of contact and impact for the system (with parameters given in Section 6.1) via Ω_c vs. e/r_c. Key: ●, operational points (with periodic impacts) selected for the purpose of error analyses.

S_1 simulation (as a result of step 5) based on the chosen residue. The trial values of β and n for the simulation that yields the least residue. These will be selected the impact damping parameters for Eq. (2)

6. Error and sensitivity analyses of the proposed estimation procedure

6.1. Error analysis

Before employing the procedure discussed in Section 5, the robustness (using error analysis) and accuracy (using sensitivity) of the procedure have to be critically studied. The purpose of these analyses is purely to get the best residue for the parameter estimation discussed in Section 7. The robustness can be better understood by the error in the residues for an ideal case, since an indirect method of comparison is being employed for the estimation process. Next S_2 simulation (with known values) is defined for conducting error and sensitivity analyses; note that S_1 is performed with trial values of damping parameters while S_2 is conducted with known values (defined as β^{S_2} and n^{S_2} with superscript S_2). The force and acceleration time-histories from simulation S_2 are used instead of the experimental data in the procedure discussed in Section 5. The residues are calculated using the simulation S_1 with $\beta^{S_1} = \beta^{S_2}$ and $n^{S_1} = n^{S_2}$. Ideally all three residues should be 0, but that is not the case due to the approximations in the estimation procedure.

The parameters selected for the cam–follower experiment for an accurate estimation of impact parameters are listed in Table 1. Inverse kinematic analysis discussed by Sundar et al. [9] is employed for the current system with the given parameters to obtain the regions on impact on an e/r_c vs. Ω_c map as shown in Fig. 3. Table 2 gives the average residue per impact, calculated using simulations S_1 and S_2 with $\beta^{S_1} = \beta^{S_2} = 24.7$ GN s m$^{-2.5}$and $n^{S_1} = n^{S_2} = 1.5$ for different values for e/r_c and Ω_c in the impact regime (shown in Fig. 3). As observed, the residues for all cases are very low, which shows that the estimation

Table 2
Comparison of average residues per impact (Λ_1, Λ_2 and Λ_3) using two simulations (S_1 and S_2) with $\beta^{S_1}=\beta^{S_2}=24.7$ GN s m$^{-2.5}$ and $n^{S_1}=n^{S_2}=1.5$.

e/r_c	Ω_c (Hz)	Average Λ_1	Average Λ_2	Average Λ_3
0.05	23	0.0056	0.0849	0.0024
0.10	18	0.0361	0.1032	0.0033
0.15	17	4.75×10^{-7}	0.0703	0.0041
0.20	16	0.78×10^{-7}	0.0728	0.0039
0.25	15	1.65×10^{-7}	0.0834	0.0043

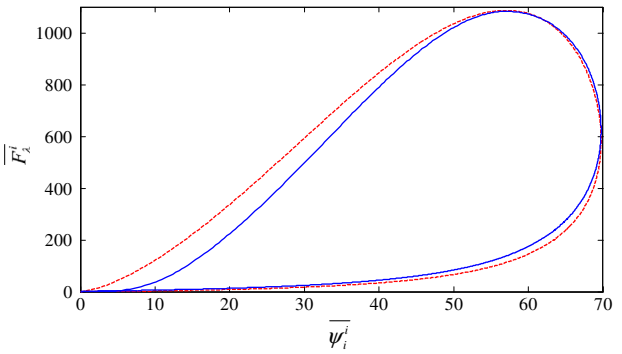

Fig. 4. Comparison of hysteresis loops for single impacts during simulation S_2 ($\beta^{S_2}=24.7$ GN s m$^{-2.5}$ and $n^{S_2}=1.5$) and simulation S_1 ($\beta^{S_1}=\beta^{S_2}$ and $n^{S_1}=n^{S_2}$) given $e/r_c=0.2$ and $\Omega_c=16$ Hz. Key: ——, simulation S_1; – – –, simulation S_2.

Table 3
Comparison of normalized average residues per impact ($\overline{\Lambda_1}$,$\overline{\Lambda_2}$, and $\overline{\Lambda_3}$) using simulation S_2 ($\beta^{S_2}=24.7$ GN s m$^{-2.5}$ and $n^{S_2}=1.5$) with $e/r_c=0.2$ and $\Omega_c=16$ Hz. (a) For different values of β^{S_1} in the proximity of β^{S_2} with constant value of $n^{S_1}=n^{S_2}$; and (b) for different values of n^{S_1} in the proximity of n^{S_2} with constant value of $\beta^{S_1}=\beta^{S_2}$.

a) For different values of β^{S_1} in the proximity of β^{S_2} with constant value of $n^{S_1}=n^{S_2}$

Normalized residue	$\beta^{S_1}=0.98\beta^{S_2}$	$\beta^{S_1}=0.99\beta^{S_2}$	$\beta^{S_1}=\beta^{S_2}$ (Ideal case)	$\beta^{S_1}=1.01\beta^{S_2}$	$\beta^{S_1}=1.02\beta^{S_2}$
$\overline{\Lambda_1}$	1.17×10^5	0.582×10^5	1	0.574×10^5	1.14×10^5
$\overline{\Lambda_2}$	0.94	0.95	1	1.05	1.06
$\overline{\Lambda_3}$	0.95	0.96	1	1.05	1.06

b) For different values of n^{S_1} in the proximity of n^{S_2} with constant value of $\beta^{S_1}=\beta^{S_2}$

Normalized residue	$n^{S_1}=0.98n^{S_2}$	$n^{S_1}=0.99n^{S_2}$	$n^{S_1}=n^{S_2}$ (Ideal case)	$n^{S_1}=1.01n^{S_2}$	$n^{S_1}=1.02n^{S_2}$
$\overline{\Lambda_1}$	17.24×10^5	8.94×10^5	1	9.42×10^5	19.2×10^5
$\overline{\Lambda_2}$	2.49	1.67	1	0.76	1.16
$\overline{\Lambda_3}$	2.07	1.52	1	0.49	0.0086

procedure is very robust for these examples. Also, it can be inferred that as e/r_c increases, Λ_1 reduces and reaches a minimum at $e/r_c=0.2$ and starts increasing again. With the increase in e/r_c the signal to noise ratio increases; hence Λ_1 reduces, but for very high values of e/r_c the system operates close to a chaotic state. The noise here might be from experimental measurements or from the numerical error (in solving equations of motion). Similar trends are not observed in the cases of Λ_2 and Λ_3. As observed, the values of Λ_1 are the lowest, followed by Λ_3, with Λ_2 being the highest. Fig. 4 compares sample hysteresis loops of simulations S_1 and S_2 for a case with $e/r_c=0.2$, where $\overline{F_\lambda^i}=F_\lambda^i/F_\lambda^*$ and $\overline{\psi_i^i}=\psi_i^i/\psi_i^*$. It is observed that for this case, a point contact with a maximum value of F_λ during impact is about three orders of magnitude greater than F_λ^* while the maximum value of ψ_i during impact is only about two orders of magnitude greater than ψ_i^*. This suggests that, contact force grows at a faster rate compared to the indentation during impact. Even for an ideal case a very good match is not found in the hysteresis loop for low values of indentation. The relative accuracies of the residues in estimating the damping parameters should not be decided from the Λ values in Table 2 but from the sensitivity of these residues to variation in β and n. Hence it is analyzed next.

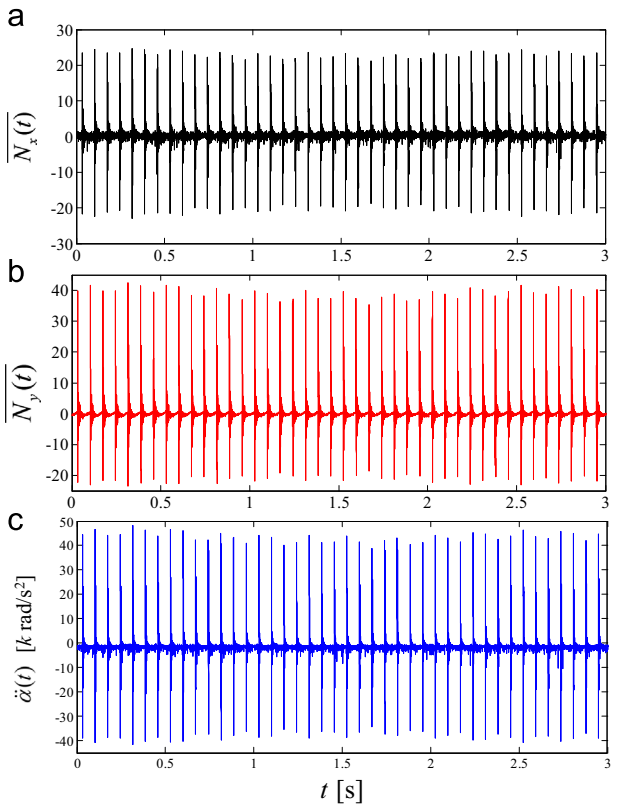

Fig. 5. Measured time histories with $e/r_c = 0.13$ and $\Omega_c = 14$ Hz (with other parameters given in Section 6.1). (a) Normalized reaction force along $\hat{e}_x$; (b) normalized reaction force along $\hat{e}_y$; and (c) angular acceleration of the follower.

6.2. Sensitivity analysis

Table 3a gives the values of normalized residues ($\overline{\Lambda}$) for simulation S_2 ($\beta^{S_2} = 24.7$ GN s m$^{-2.5}$ and $n^{S_2} = 1.5$) and simulation S_1 with $n^{S_1} = n^{S_2}$ with different values of β^{S_1} in close proximity of β^{S_2}. The residues are normalized based on its value when $\beta^{S_1} = \beta^{S_2}$. The sensitivity of the residues to a change in β can be understood from this table. It can be easily inferred that $\overline{\Lambda}_1$ has a very high sensitivity even to a very small change in the value of β compared to that of $\overline{\Lambda}_2$ and $\overline{\Lambda}_3$. Also, ideally, $\overline{\Lambda}$ should be lowest for $\beta^{S_1} = \beta^{S_2}$, but that is not the case with $\overline{\Lambda}_2$ and $\overline{\Lambda}_3$, which may lead to an incorrect estimation of β. A similar analysis is performed to study the sensitivity of residues to a change in n and the result is shown in Table 3b. Compared to the other two residues, $\overline{\Lambda}_1$ is more sensitive to changes in n. Also, unlike $\overline{\Lambda}_1$, the lowest value does not occur at $n^{S_1} = n^{S_2}$ for $\overline{\Lambda}_2$ and $\overline{\Lambda}_3$. Thus Λ_1 is more accurate than other residues, and hence it will be used in the estimation of the impact damping model for the experimental system. Note that the estimation procedure using Λ_1 uses only the measured acceleration and not the forces.

The reasons for the inaccuracies of Λ_2 and Λ_3 are as follows. The residue Λ_2 is inaccurate because it is based on the calculated F_λ during the impact which is for a very short time period. Since Λ_2 uses the integration of F_λ over time even a small error in the estimation of F_λ is magnified in the residue calculation. The residue Λ_3 is based on a hysteresis loop where F_λ is plotted against ψ_i which is very small in magnitude (< 50 μm) during contact compared to the magnitude of ψ_i (~ 20 mm) during non-contact. Moreover, $\psi_i(t)$ is calculated using $\alpha(t)$ which has some error caused by numerical integration. Hence, even a small error in the estimation of ψ_i results in a very high error in the hysteresis loop. Thus, the sampling rate of data acquisition must be much higher (than the one which is used in this experiment) to employ Λ_2 or Λ_3 in the estimation procedure.

7. Estimation of impact damping parameters from measurements

The procedure discussed in Section 5.2 had been employed to estimate the impact damping model parameters for the experimental system shown in Fig. 1. The experiment was conducted for a given value of e/r_c and Ω_c is slowly increased until one impact per revolution of the cam is achieved. The distinct impacts are visible in the time histories of the normalized measured reaction forces ($\overline{N_x(t)} = N_x(t)/F^*_\lambda, \overline{N_y(t)} = N_y(t)/F^*_\lambda$) and measured acceleration shown in Fig. 5 from which T is obtained and its relationship with $1/\Omega_c$ is verified. Fig. 6 shows normalized reaction forces and acceleration data

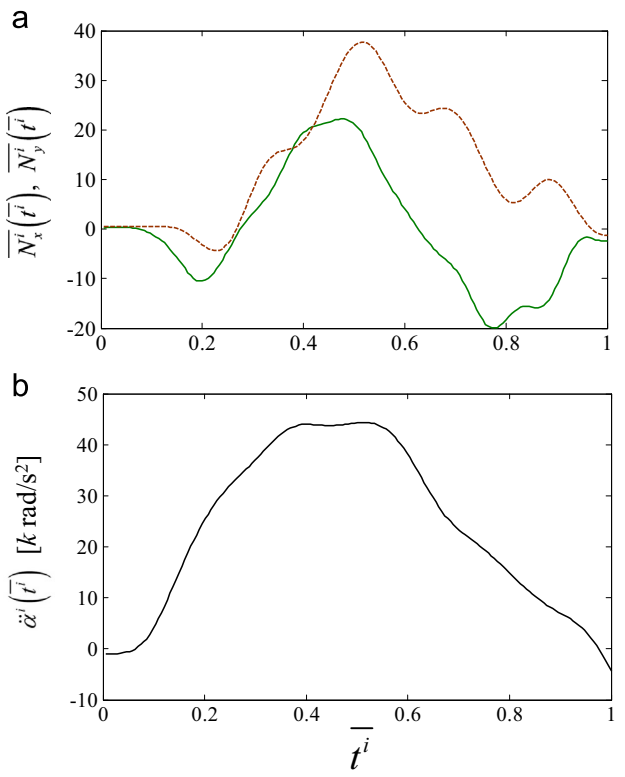

Fig. 6. Sample measured forces and acceleration during a contact sub-event. (a) Reaction forces; and (b) angular acceleration. Key: ——, $\overline{N_x^i}(\overline{t^i})$; – – –, $\overline{N_y^i}(\overline{t^i})$.

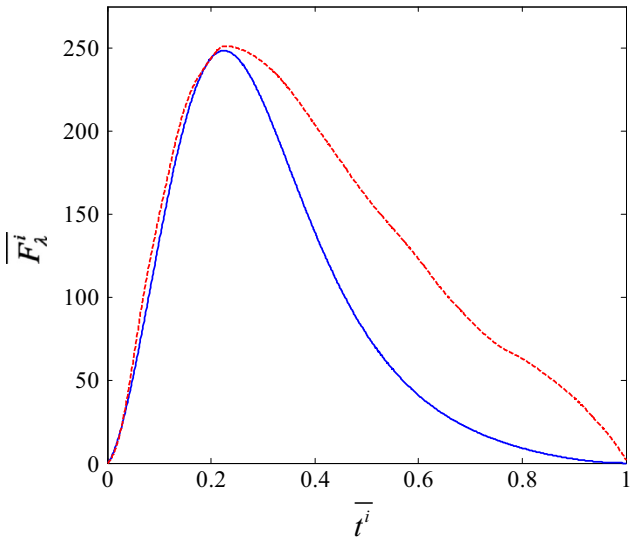

Fig. 7. Comparison of the hysteresis loops from measured data of Fig. 6 and simulation S_1 (with impact damping model; $\beta^{S_1}=49.3$ GN s m$^{-2.5}$ and $n^{S_1}=1.5$). Key: – – –, measured; ——, simulation S_1.

measured during the contact sub-event of a sample impact from the experiment with $e/r_c=0.13$ and $\Omega_c=14.05$ Hz (with measured $T=0.0712$ s), with all other parameters being the same as given in Section 6.1, where the normalized time is given by $\overline{t_i}=t_i/t_a^i$. The values of the impact damping parameters identified using minimization of $\Lambda_1$are $\beta=92.6$ GN s m$^{-2.55}$ and $n=1.55$ (note that the unit of β depends on the numerical value of n, since $\beta|\psi_i|^n\dot{\psi}_i$ should have the units of force). The estimated value of n from the experimental data agrees closely with $n=1.5$ which would fit the contact force formulation of $F_\lambda=F_k\left(1+\kappa\dot{\delta}\right)$., which is used by many researchers [21,23–25]. Hence the same procedure is followed by forcing $n=1.5$ and β is evaluated as 49.3 GN s m$^{-2.5}$. Fig. 7 shows a comparison of the contact forces of sample impact from the experimental

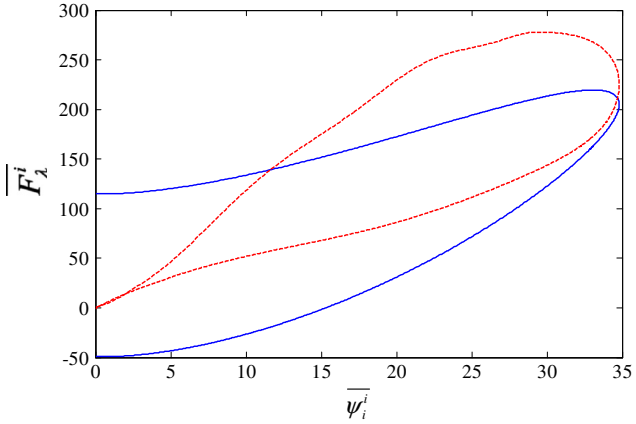

Fig. 8. Comparison of the hysteresis loops from measured data of Fig. 6 and simulation S_1 (with viscous damping model; $n^{S_1}=0$ and $\beta^{S_1}=1.47$ kN s/m) Key: ▬ ▬ ▬, measured; ▬▬▬, simulation S_1.

data and the simulation S_1 (with $\beta^{S_1}=49.3$ GN s m$^{-2.5}$ and $n^{S_1}=1.5$). As can be inferred, though the damping parameters have been selected based on the α_m there is a good match in the shape and peak value of the contact force. Also it is very important to note that for a very small change in the value of n (about 3%) there is a very significant change in the estimated value of β of about 46%. Hence n is more critical than β in the impact damping formulation. Instead, if n is taken as 1.45, β is estimated as 29.3 GN s m$^{-2.45}$. The experiment was repeated with different values of e/r_c and Ω_c and the same estimation procedure was been followed to obtain β and n values. Since the estimated values of β and n were consistent, the repeatability of the experiment and the accuracy of the estimation procedure are validated. Also, Sundar et al. [9] estimated the values of κ for a similar system under dry conditions ranging from 3.25 s/m to 4.25 s/m which are comparable to $\kappa=3.8$ s/m to 6.5 s/m (for $n=1.45$ to 1.5, respectively) for the current system.

To check if a viscous damping model can be used to represent an impact event, n is forced to be 0 and the same procedure is followed to obtain $\beta=1.47$ kN s/m. A sample hysteresis loop comparing the experimental data and simulation S_1 (with $n^{S_1}=0$ and $\beta^{S_1}=1.47$ kN s/m) for the same is shown in Fig. 8. As it can be easily inferred there is a very clear variation in the shape of the hysteresis loops. Furthermore, F_λ goes to a negative value (tensile force) for part of the loop which is impractical; hence a viscous damping model is not a good approximation to model impacts.

8. Equivalent coefficient of restitution and justification of damping parameters

8.1. Governing equation

An equivalent coefficient of restitution ξ is defined by the ratio of velocity of recession to the velocity of approach (v_a), and for the current system it is defined as follows:

$$\xi = -\frac{\dot{\psi}_i^a}{\dot{\psi}_i^b}. \tag{24}$$

Though a few prior researchers [9,35] have assumed ξ to be a constant value, a more generalized model of the form is considered in this article as:

$$\xi = 1-\gamma v_a. \tag{25}$$

Here, ξ decreases with v_a at a constant rate of γ, as suggested by Hunt and Crossley [24]. Instead of using Eq. (16) in the contact regime (for the contact mechanics formulation), this ξ formulation is used to calculate the state of the system after the impact (with superscript a) using the state of the system just before impact (with superscript b). Since $v_a=\left|\dot{\psi}_i^b\right|$, Eq. (25) is rewritten as:

$$\xi = 1-\gamma\left|\dot{\psi}_i^b\right|. \tag{26}$$

From Eqs. (24) and (26) the velocity of separation is calculated as $\dot{\psi}_i^a = -\dot{\psi}_i^b\left(1-\gamma\left|\dot{\psi}_i^b\right|\right)$. The state of the system before impact is obtained from the response of the system in the non-contact regime when $\psi_i(t)=0$. Rearranging Eq. (7) $\dot{\alpha}^a$ is

Table 4
Error in the estimation of ξ model using time histories from simulation S_3 ($\gamma^{S_3}=0.8$ s/m).

e/r_c	Ω_c (Hz)	Estimated γ (s/m)	% error $=\left\lvert\frac{\gamma-\gamma^r}{\gamma^r}\right\rvert\times 100$
0.05	23	0.8	0
0.10	18	0.799	0.13
0.15	17	0.8	0
0.20	16	0.76	5.0
0.25	15	0.8	0

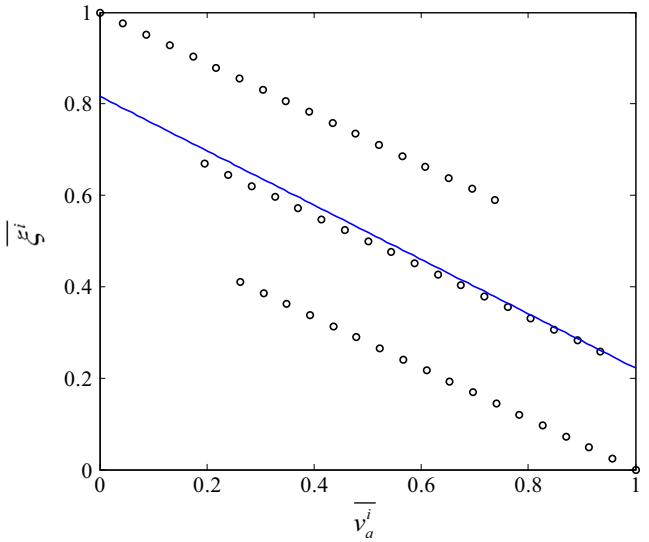

Fig. 9. Variation in estimated $\overline{\xi^i}$ with $\overline{\psi_i^b}$ given $e/r_c=0.10$ and $\Omega_c=18$ Hz. Key: ○, simulation S_3 ($\gamma^{S_3}=0.8$ s/m); ——, estimated $\overline{\xi}$ model with $\gamma=0.80$ s/m (using least square curve-fit).

calculated as

$$\dot{\alpha}^a=\frac{\dot{\psi}_i^a+e\ \cos\left(\alpha^a+\Theta^a\right)\dot{\Theta}}{\chi^0\ \cos\left(\alpha^a-\alpha^0\right)-\left(r_c+0.5w_b+2r_d\right)\sin\left(\alpha^a-\alpha^0\right)+e\left[\cos\left(\alpha^a+\Theta^0\right)-\ \cos\left(\alpha^a+\Theta^a\right)\right]}. \tag{27}$$

Mathematically, in ξ formulation the system is in contact just for a single instant, and hence α^a and Θ^a are approximated by their corresponding values before impact.

8.2. Estimation of the equivalent ξ model

Unlike the estimation of impact damping, a direct method can be employed to estimate ξ. Since the state of the system just before impact (with superscript b) is needed for this purpose, it is calculated using a numerical backward difference technique as given by the following equations,

$$\alpha^b=\alpha^i(-\tau)=\alpha^i(0)-\tau\dot{\alpha}^i(0), \tag{28a}$$

$$\dot{\alpha}^b=\dot{\alpha}^i(-\tau)=\dot{\alpha}^i(0)-\tau\ddot{\alpha}^i(0), \tag{28b}$$

$$\Theta^b=\Theta^i(-\tau)=\Theta^i(0)-\tau\dot{\Theta}^i(0) \tag{28c}$$

Velocity of approach ($\dot{\psi}_i^b$) is calculated from Eq. (7) by replacing $\alpha(t)$, $\dot{\alpha}(t)$ and $\Theta(t)$ with α^b, $\dot{\alpha}^b$ and Θ^b, respectively, while the velocity of separation ($\dot{\psi}_i^a$) is the value of $\dot{\psi}_i^i(t)$ when $\dot{\alpha}^i(t)$ reaches maximum. Using Eq. (25), ξ^i is estimated for each impact. From ξ^i and($\dot{\psi}_i^a$), γ is identified using least square curve-fitting technique.

An analysis similar to the one discussed in Section 6.1 has been performed to evaluate the error in the estimation of ξ. Simulation S_3 is defined for a coefficient of restitution model similar to S_1 and S_2 simulations for the impact damping model. Force and acceleration time histories from S_3, with known $\gamma^{S_3}=0.8$ s/m (other parameters are the same as given in Section

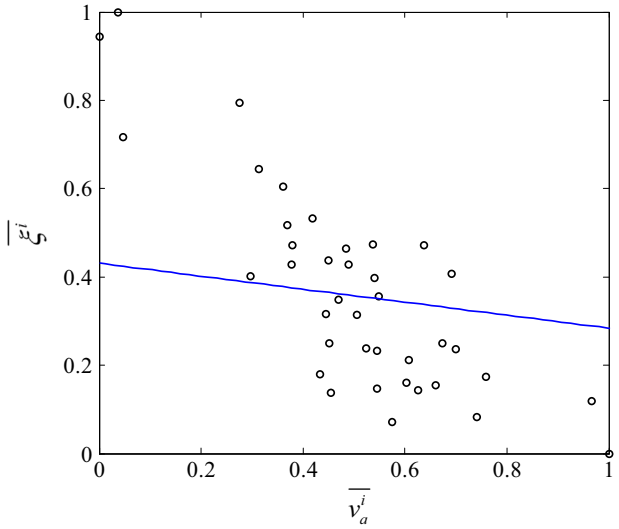

Fig. 10. Variation in estimated $\overline{\xi^i}$ with $\overline{\psi_i^p}$ for the experimental data of Fig. 5. Key: ○, experimental data; ——, estimated $\overline{\xi}$ model with $\gamma=0.76$ s/m (using least square curve-fit).

6.1) is taken as reference. The ξ^i is estimated for each impact for cases with different e/r_c. The estimated γ and the % error associated with its estimation are given in Table 4. It is inferred from the magnitude of errors that this procedure yields very accurate γ for all the cases of e/r_c. Fig. 9 shows the variation of ξ^i with v_a^i on a normalized basis (on a scale of 0–1), for a sample case with $e/r_c=0.1$ and $\Omega_c=18$ Hz. The normalized ξ^i and v_a^i are calculated as follows, where 'min' is a function that returns the minimum value of a set of inputs,

$$\overline{\xi^i}=\frac{\xi^i-\min(\xi)}{\max(\xi)-\min(\xi)}, \tag{29}$$

$$\overline{v_a^i}=\frac{v_a^i-\min(v_a)}{\max(v_a)-\min(v_a)}. \tag{30}$$

Fig. 9 also shows the ξ model estimated using the least square curve-fitting technique with $\gamma=0.80$ s/m.

For the same measured data (shown in Fig. 5), ξ^i is estimated for each impact using the procedure (discussed in Section 8.2) and the results are shown on a normalized basis (using (Eqs. (29) and 30)) in Fig. 10. The least square curve-fitting technique was applied to estimate γ as 0.76 s/m using the measured data, and line fit is also shown in Fig. 10. The average of the estimated ξ for all impacts is 0.75 with a velocity of approach of 0.34 m/s which is similar to the value of $\xi=0.65$ reported by Seifried et al. [33] for v_a of 0.3 m/s, under similar impacting conditions.

8.3. *Justification of the estimated impact damping parameters*

The relationship between coefficient of restitution and impact damping formulations has been derived by Hunt and Crossley [24] for vibroimpacts. Using this formula the equivalent β for the estimated γ (0.758 s/m) is obtained as 9.1 GN s m$^{-2.5}$, which is comparable to the values estimated experimentally in Section 7 (49.3 GN s m$^{-2.5}$ for $n=1.5$ and 29.3 GN s m$^{-2.45}$ for $n=1.45$). Some reasons for the difference between the β values are: a) Hunt and Crossley [24] derived the relationship for vibroimpacts under dry conditions assuming pure metal to metal contact, but the experiments were under lubricated condition; b) even a small change in n value affects β significantly; and c) the ξ concept has an inherent drawback [9,23] and hence the experimental estimation of γ might have some inaccuracies. Taking these points into consideration, the estimated values for impact damping parameters are justified on an order of magnitude basis.

9. Conclusion

The chief contribution of this study is the design of a controlled new cam–follower experiment (having periodic impacts to accurately measure dynamic forces and motion during impacts) along with the development of a computational method to estimate the impact damping parameters from measurements. Related minor contributions are as follows. First, a novel time-domain based technique to estimate $\alpha(t)$ is developed, which minimizes the effect of errors associated with the numerical integration. Second, a new signal processing procedure is developed which utilizes only the measured accelerations to estimate the impact damping parameters. Finally, an improved understanding of the impact damping is obtained

by answering all the relevant questions (stated in Section 2) in the context of a cam–follower system. The proposed signal processing procedure (using Λ_1) does not require any force measurements; hence it could be extended to other mechanical systems. However, the chief limitation of this study is the indirect estimation of impact damping model; thus future work may be directed towards development of a direct method, possibly for a line contact.

Acknowledgment

The authors gratefully acknowledge the Vertical Lift Consortium, Inc., Smart Vehicle Concepts Center (www.SmartVehicleCenter.org) and the National Science Foundation Industry/University Cooperative Research Centers program (www.nsf.gov/eng/iip/iucrc) for partially supporting this research.

References

[1] R. Singh, H. Xie, R.J. Comparin, Analysis of automotive neutral gear rattle, J. Sound Vib. 131 (1989) 177–196.
[2] M.Y. Wang, R. Manoj, W. Zhao, Gear rattle modelling and analysis for automotive manual transmissions, Proc. Inst. Mech. Eng. Part D: J. Automob. Eng. 215 (2001) 241–258.
[3] S. Theodossiades, S. Natsiavas, Periodic and chaotic dynamics of motor-driven gear-pair systems with backlash, Chaos Solitons Fractals 12 (2001) 2427–2440.
[4] T. Sakai, Y. Doi, K. Yamamoto, T. Ogasawara, M. Narita, Theoretical and experimental analysis of rattling noise of automotive gearbox, Society of Automotive Engineers, 1981, SAE paper 810773.
[5] K. Karagiannis, F. Pfeiffer, Theoretical and experimental investigations of gear-rattling, Nonlinear Dyn. 2 (1991) 367–387.
[6] F.Y. Chen, A survey of the state of the art of cam system dynamics, Mech. Mach. Theory 12 (1977) 201–224.
[7] R. Alzate, M. di Bernardo, G. Giordano, G. Rea, S. Santini, Experimental and numerical investigation of coexistence, novel bifurcations, and chaos in a cam–follower system, SIAM J. Appl. Dyn. Syst. 8 (2009) 592–623.
[8] R. Alzate, M. di Bernardo, U. Montanaro, S. Santini, Experimental and numerical verification of bifurcations and chaos in cam–follower impacting systems, Nonlinear Dyn. 50 (2007) 409–429.
[9] S. Sundar, J.T. Dreyer, R. Singh, Rotational sliding contact dynamics in a non-linear cam–follower system as excited by a periodic motion, J. Sound Vib. 332 (2013) 4280–4295.
[10] S.H. Cho, S.T. Ahn, Y.H. Kim, A simple model to estimate the impact force induced by piston slap, J. Sound Vib. 255 (2002) 229–242.
[11] R. Wilson, J.N. Fawcett, Dynamics of the slider-crank mechanism with clearance in the sliding bearing, Mech. Mach. Theory 9 (1974) 61–80.
[12] E.E. Ungar, D. Ross, Vibrations and noise due to piston-slap in reciprocating machinery, J. Sound Vib. 2 (1965) 132–146.
[13] G.S. Whiston, Impacting under harmonic excitation, J. Sound Vib. 67 (1979) 179–186.
[14] R. Palej, J. Niziol, On a direct method of analyzing impacting mechanical systems, J. Sound Vib. 108 (1986) 191–198.
[15] R.J. Comparin, R. Singh, Non-linear frequency response characteristics of an impact pair, J. Sound Vib. 134 (1989) 259–290.
[16] C.N. Bapat, N. Popplewell, K. McLachlan, Stable periodic motions of an impact-pair, J. Sound Vib. 87 (1983) 19–40.
[17] C.K. Sung, W.S. Yu, Dynamics of a harmonically excited impact damper: Bifurcations and chaotic motion, J. Sound Vib. 158 (1992) 317–329.
[18] S. Chatterjee, A.K. Mallik, Bifurcations and chaos in autonomous self-excited oscillators with impact damping, J. Sound Vib. 191 (1996) 539–562.
[19] D.M. Egle, An investigation of an impact vibration absorber, J. Eng. Ind. 89 (1967) 653–657.
[20] S.W. Shaw, P.J. Holmes, A periodically forced impact oscillator with large dissipation, J. Appl. Mech. 50 (1983) 849–857.
[21] C. Padmanabhan, R. Singh, Dynamics of a piecewise non-linear system subject to dual harmonic excitation using parametric continuation, J. Sound Vib. 184 (1995) 767–799.
[22] D. Zhang, W.J. Whiten, The calculation of contact forces between particles using spring and damping models, Powder Technol. 88 (1996) 59–64.
[23] M.A. Veluswami, F.R.E. Crossley, G. Horvay, Multiple impacts of a ball between two plates-part 2: mathematical modelling, J. Eng. Ind. 97 (1975) 828–835.
[24] K.H. Hunt, F.R.E. Crossley, Coefficient of restitution interpreted as damping in vibroimpact, J. Appl. Mech. 42 (1975) 440.
[25] R.C. Azar, F.R.E. Crossley, Digital simulation of impact phenomenon in spur gear systems, J. Eng. Ind. 99 (1977) 792–798.
[26] G.G. Gray, K.L. Johnson, The dynamic response of elastic bodies in rolling contact to random roughness of their surfaces, J. Sound Vib. 22 (3) (1972) 323–342.
[27] M.A. Veluswami, F.R.E. Crossley, Multiple impacts of a ball between two plates-part 1: some experimental observations, J. Eng. Ind. 97 (1975) 820–827.
[28] ⟨http://gbr.sika.com⟩, (accessed 15.08.13).
[29] M. Eriten, A.A. Polycarpou, L.A. Bergman, Development of a lap joint fretting apparatus, Exp. Mech. 51 (8) (2011) 1405–1419.
[30] PCB Piezotronics Inc., Sensors for acceleration, shock, vibration and acoustic measurements: Product catalog (Model 350B02), Depew, NY. ⟨http://www.pcb.com⟩, 2004 (accessed 15.08.13).
[31] LMS instruments. LMS SCADAS III data acquisition front-end, Breda, The Netherlands. ⟨http://www.lmsintl.com⟩, 2008 (accessed 15.08.13).
[32] P.J. Davis, P. Rabinowitz, Methods of Numerical Integration, Courier Dover Publications, Mineola, New York, 2007.
[33] R. Seifried, W. Schiehlen, P. Eberhard, Numerical and experimental evaluation of the coefficient of restitution for repeated impacts, Int. J. Impact Eng. 32 (2005) 508–524.